

# Layer-by-Layer Growth of $\text{CH}_3\text{NH}_3\text{PbI}_{3-x}\text{Cl}_x$ for Highly Efficient Planar Heterojunction Perovskite Solar Cells

Yonghua Chen, Tao Chen, and Liming Dai\*

Owing to their broad spectral absorption,<sup>[1]</sup> high charge-carrier mobility,<sup>[2]</sup> small exciton binding energy ( $\approx 50$  meV),<sup>[3]</sup> and long exciton diffusion length,<sup>[4,5]</sup> the organic-inorganic hybrid methylammonium lead halide perovskites (e.g.,  $\text{CH}_3\text{NH}_3\text{PbX}_3$ , X = Cl, Br, I), have recently attracted enormous attention for thin-film photovoltaics.<sup>[6–10]</sup> High-performance perovskite solar cells in both mesoporous scaffold and planar heterojunction architectures have been reported to show power conversion efficiencies (PCEs) over 19% with some dedicated energy-level engineering.<sup>[11–16]</sup> Since conventional spin-casting has been currently used to form the perovskite active layer from a mixture of  $\text{PbX}_2$  and  $\text{CH}_3\text{NH}_3\text{X}$  in a common solvent (e.g., dimethylformamide (DMF)), the poor solubility of  $\text{PbX}_2$  usually leads to large morphological variations (even with pinholes) for the solution-cast perovskite layer, and hence unstable device performance. Despite the recent rapid increase in PCEs of various perovskite solar cells,<sup>[15–21]</sup> therefore, morphological control is a bottleneck in further development of the state-of-the-art perovskite solar cells. In this context, a sequential deposition method has been recently reported for the formation of the perovskite by first introducing lead iodide ( $\text{PbI}_2$ ) into a nanoporous titanium dioxide film, followed by exposing it to a solution of  $\text{CH}_3\text{NH}_3\text{I}$  to produce the perovskite layer without the uncontrollable precipitation of the perovskite in the casting solution.<sup>[11]</sup> Although this two-step method permitted a much better control over the perovskite morphology (and hence a high PCE of approximately 15%) with respect to the one-step solution casting, it is still difficult to control the morphology of  $\text{PbI}_2$  film made from solution casting due to its intrinsically poor solubility, and the porous metal oxide film is needed for the surface-assisted complete transformation of  $\text{PbI}_2$  and  $\text{CH}_3\text{NH}_3\text{I}$  into the perovskite layer.

Compared with  $\text{CH}_3\text{NH}_3\text{PbI}_3$ ,  $\text{CH}_3\text{NH}_3\text{PbI}_{3-x}\text{Cl}_x$  perovskites possess a higher charge carrier mobility and longer exciton diffusion length<sup>[2,4]</sup> so that it is more attractive for fabrication of perovskite solar cells, especially in flat architectures. So far, most of the  $\text{CH}_3\text{NH}_3\text{PbI}_{3-x}\text{Cl}_x$  perovskite layers reported were obtained by solution casting from a mixture of  $\text{PbCl}_2$  and  $\text{CH}_3\text{NH}_3\text{I}$  (1:3, mol/mol) in DMF<sup>[22,23]</sup> except the work reported by Liu et al.,<sup>[12]</sup> in which a dual-source vapor deposition method was used to deposit the perovskite layer onto

a  $\text{TiO}_2$ -coated fluorine-doped tin oxide.<sup>[12]</sup> The solution casting approach often leads to non-uniform film morphologies to limit the perovskite device performance. Here, we developed a layer-by-layer approach to uniform  $\text{CH}_3\text{NH}_3\text{PbI}_{3-x}\text{Cl}_x$  perovskite flat films for high-performance perovskite solar cells with an improved stability. Environmental instability is one of the major problems limited practical application of perovskite solar cells, this study represents an important step forward in developing high-performance and stable perovskite solar cells.

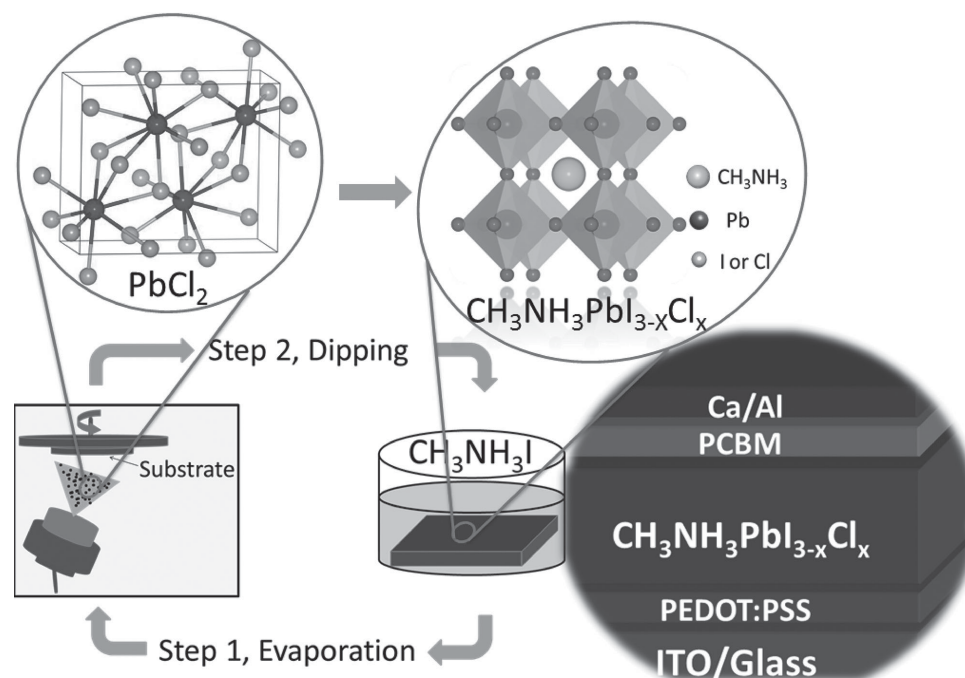
Briefly, a thin (50 nm) layer of  $\text{PbCl}_2$  was first deposited by thermal evaporation onto a poly(3,4-ethylenedioxythiophene):poly(styrenesulfonate) (PEDOT:PSS) layer pre-coated on an indium tin oxide (ITO)/glass substrate (Figure 1). Subsequent dipping of the  $\text{PbCl}_2$  into a solution of  $\text{CH}_3\text{NH}_3\text{I}$  in 2-propanol ( $10 \text{ mg mL}^{-1}$ ) transferred it into a layer of  $\text{CH}_3\text{NH}_3\text{PbI}_{3-x}\text{Cl}_x$  perovskite. Similarly, a second  $\text{PbCl}_2$  layer (50 nm) was thermally evaporated onto the newly formed  $\text{CH}_3\text{NH}_3\text{PbI}_{3-x}\text{Cl}_x$  perovskite film, followed by dipping into the  $\text{CH}_3\text{NH}_3\text{I}$  solution to form the second layer of  $\text{CH}_3\text{NH}_3\text{PbI}_{3-x}\text{Cl}_x$  perovskite intimately contacted with the underlying preformed  $\text{CH}_3\text{NH}_3\text{PbI}_{3-x}\text{Cl}_x$  perovskite layer, and the process was repeated (Steps 1 and 2, Figure 1) several times to form an interface-free uniform  $\text{CH}_3\text{NH}_3\text{PbI}_{3-x}\text{Cl}_x$  perovskite layer of a desirable total thickness for outstanding photovoltaic performance. We found that the thermally evaporated  $\text{PbCl}_2$  film, though somewhat dense, could be converted into the  $\text{CH}_3\text{NH}_3\text{PbI}_{3-x}\text{Cl}_x$  perovskite once came into contact with the  $\text{CH}_3\text{NH}_3\text{I}$  solution, allowing for a relatively feasible control of the perovskite morphology with respect to previously reported one-step mixture solution casting or two-step solution casting with the first formation of a  $\text{PbI}_2$  layer.<sup>[11]</sup> In conjugation with appropriate organic charge-transporting layers, the layer-by-layer approach enabled us to effectively fabricate planar heterojunction perovskite solar cells with a PCE as high as 15.12% and flexible perovskite devices of a record high PCE of 12.25% via both forward-to-reverse bias scans without hysteresis (vide infra).

Figure 1 schematically shows the layer-by-layer process for fabrication of the  $\text{CH}_3\text{NH}_3\text{PbI}_{3-x}\text{Cl}_x$  perovskite solar cells while detailed device construction and characterization are given in Methods. It is critical to control the  $\text{PbCl}_2$  thickness (50 nm) for a complete transformation into a uniform  $\text{CH}_3\text{NH}_3\text{PbI}_{3-x}\text{Cl}_x$  perovskite layer by reacting with  $\text{CH}_3\text{NH}_3\text{I}$ . This is because a thin film of  $\text{PbCl}_2$  could lead to the formation of an inhomogeneous  $\text{CH}_3\text{NH}_3\text{PbI}_{3-x}\text{Cl}_x$  perovskite layer with pinholes (Supporting Information, Figure S1) whereas a thick  $\text{PbCl}_2$  layer would cause an incomplete conversion of the compact  $\text{PbCl}_2$  film into the  $\text{CH}_3\text{NH}_3\text{PbI}_{3-x}\text{Cl}_x$  perovskite on exposure to the  $\text{CH}_3\text{NH}_3\text{I}$  solution (Supporting Information, Figure S2),<sup>[11,24]</sup> leading to the formation of undesirable  $\text{PbCl}_2$  interfaces within the resultant  $\text{CH}_3\text{NH}_3\text{PbI}_{3-x}\text{Cl}_x$  perovskite formed by the layer-by-layer approach and thus the poor performance (Supporting

Dr. Y. Chen, Dr. T. Chen, Prof. L. Dai  
Center of Advanced Science and Engineering  
for Carbon (Case4Carbon)  
Department of Macromolecular Science and  
Engineering, Case School of Engineering  
Case Western Reserve University  
10900 Euclid Avenue, Cleveland, Ohio 44106, USA  
E-mail: liming.dai@case.edu



DOI: 10.1002/adma.201404147



**Figure 1.** Schematic representation of the layer-by-layer deposition for device fabrication. The procedure and the resultant device structure.

Information, Figure S3). Although a prolonged dipping of the  $\text{PbCl}_2$  coating in the  $\text{CH}_3\text{NH}_3\text{I}$  solution in 2-propanol can enhance its conversion to  $\text{CH}_3\text{NH}_3\text{PbI}_{3-x}\text{Cl}_x$  perovskite, the long dipping time could cause the  $\text{CH}_3\text{NH}_3\text{PbI}_{3-x}\text{Cl}_x$  perovskite crystals to increase size up to several micrometers with a concomitant rough surface (Supporting Information, Figure S4), leading to a poor device performance with the prolonged dipping time (Supporting Information, Figure S5). An increase in the concentration of  $\text{CH}_3\text{NH}_3\text{I}$  from 30 to 60  $\text{mg mL}^{-1}$  could enhance the device performance due to a more complete conversion at a higher  $\text{CH}_3\text{NH}_3\text{I}$  concentration (Supporting Information, Figure S6). At a high  $\text{CH}_3\text{NH}_3\text{I}$  concentration, however, the unreacted  $\text{CH}_3\text{NH}_3\text{I}$  residues (Supporting Information, Figure S7) could also cause detrimental effects on the charge transport and charge recombination in the perovskite film. Therefore, we have optimized the fabrication conditions to use a relatively thin  $\text{PbCl}_2$  (e.g., 50 nm), low concentration of  $\text{CH}_3\text{NH}_3\text{I}$  (e.g., 10  $\text{mg mL}^{-1}$ ), and short dipping time (e.g., 40 s) for the formation of  $\text{CH}_3\text{NH}_3\text{PbI}_{3-x}\text{Cl}_x$  perovskite layer in the high-performance solar cells studied in this work (vide infra).

Dipping the  $\text{PbCl}_2$  coating into a solution of  $\text{CH}_3\text{NH}_3\text{I}$  in 2-propanol (10  $\text{mg mL}^{-1}$ ) caused an immediate color change from colorless to yellow, indicating the formation of  $\text{CH}_3\text{NH}_3\text{PbI}_{3-x}\text{Cl}_x$  perovskite. As can be seen in Figure S8 in the Supporting Information, the “multilayered”  $\text{CH}_3\text{NH}_3\text{PbI}_{3-x}\text{Cl}_x$  perovskite film showed a gradual color change from the greenish yellow to dark brown with increasing layer number. The formation process of the “multilayered” perovskite was also monitored by optical absorption, X-ray diffraction (XRD), X-ray photoelectron spectroscopy (XPS), and top-view scanning electron microscopic (SEM) images (Figure 2). A typical absorption spectrum with an onset at 770 nm characteristic of the  $\text{CH}_3\text{NH}_3\text{PbI}_{3-x}\text{Cl}_x$  perovskite was evident in Figure 2a.<sup>[25]</sup>

This, together with the largely lack of optical absorption features intrinsically associated with the  $\text{PbCl}_2$  layer (Supporting Information, Figure S9), suggests an almost complete transformation of the  $\text{PbCl}_2$  layer into  $\text{CH}_3\text{NH}_3\text{PbI}_{3-x}\text{Cl}_x$  perovskite. A continuous increase from 1 layer (L) to 8L for the “multilayered” perovskite caused an increase in the absorption across the entire spectral range, especially over long wavelengths, providing an important advantage for photovoltaic applications. The saturated absorption over 6L suggests the achievement of a limited layer thickness while the constant absorption onset for all the perovskite samples with different layer numbers reveals a layer-number-independent optical bandgap.

Further evidence for the complete conversion of  $\text{PbCl}_2$  layer into the  $\text{CH}_3\text{NH}_3\text{PbI}_{3-x}\text{Cl}_x$  perovskite film came from XRD measurements (Figure 2b). Upon reacting with the  $\text{CH}_3\text{NH}_3\text{I}$  solution, the most intense XRD peak at  $22.68^\circ$  characteristic of  $\text{PbCl}_2$  disappeared, which was accompanied by the concomitant appearance of the (110), (220), and (330) diffraction peaks at  $13.4^\circ$ ,  $27.56^\circ$ , and  $42.48^\circ$ , respectively, arising from the tetragonal  $\text{CH}_3\text{NH}_3\text{PbI}_{3-x}\text{Cl}_x$  perovskite (Figure 2b).<sup>[12]</sup> As expected, the intensities of these newly appeared diffraction peaks of the  $\text{CH}_3\text{NH}_3\text{PbI}_{3-x}\text{Cl}_x$  perovskite film increased gradually with increasing the layer number and then saturated over 6L, in a good consistency with the optical absorption spectra shown in Figure 2a. Compared with a one-step solution-cast  $\text{CH}_3\text{NH}_3\text{PbI}_{3-x}\text{Cl}_x$  perovskite film, the enhanced (330) peak with respect to (110) and (220) peaks seen in Figure S10 in the Supporting Information for the layer-by-layer deposited  $\text{CH}_3\text{NH}_3\text{PbI}_{3-x}\text{Cl}_x$  perovskite coating indicates an increased orientation of crystalline domains by our layer-by-layer approach. The uniform  $\text{CH}_3\text{NH}_3\text{PbI}_{3-x}\text{Cl}_x$  perovskite film with oriented crystalline domains (Figure 2c and Figure S11, Supporting Information) thus ensures a high charge mobility necessary

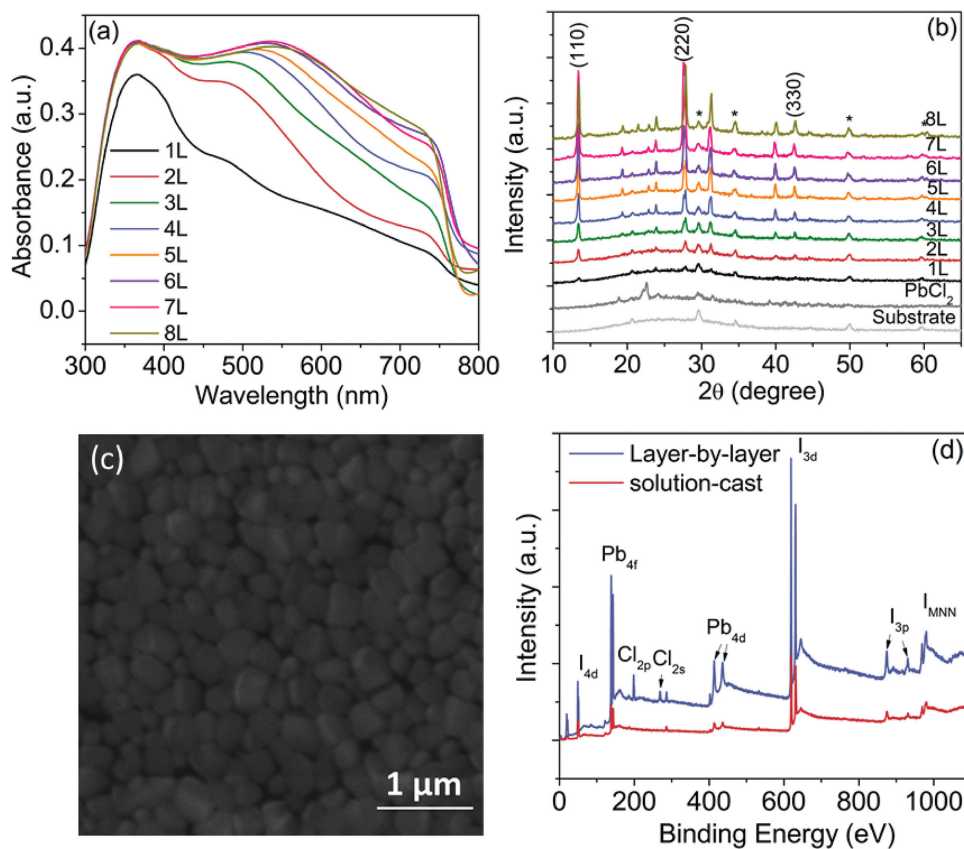


**Figure 2.** Characteristics of  $\text{CH}_3\text{NH}_3\text{PbI}_{3-x}\text{Cl}_x$  perovskite films from layer-by-layer deposition. a) UV-vis absorbance spectra of the perovskite films with different layer numbers. b) XRD patterns of the perovskite films with different layer numbers. The corresponding profile for  $\text{PbCl}_2$  was also shown as a reference. c) A top-view SEM image of the 7L  $\text{CH}_3\text{NH}_3\text{PbI}_{3-x}\text{Cl}_x$  perovskite film. d) An XPS survey spectrum of the  $\text{CH}_3\text{NH}_3\text{PbI}_{3-x}\text{Cl}_x$  perovskite film fabricated from the layer-by-layer (7L) and one-step solution-cast approach.

for high-performance solar cells. In contrast, the perovskite films with a similar thickness ( $\approx 330$  nm) fabricated by conventional one-step solution casting are often non-uniform with many pinholes (Figure S12, Supporting Information), as also reported in literature.<sup>[22,25]</sup> The  $\text{PbCl}_2$  layers formed by thermal evaporation and solution casting also exhibited quite different morphologies, as shown in Figure S13 in the Supporting Information. The compact morphologies for the  $\text{CH}_3\text{NH}_3\text{PbI}_{3-x}\text{Cl}_x$  perovskite film and its  $\text{PbCl}_2$  precursor from the layer-by-layer approach can effectively avoid the direct contact between the hole-transporting layer (e.g., PEDOT:PSS) and electron-transporting layer (e.g., [6,6]-phenyl-C61-butyric acid methyl ester, PCBM), and hence a remarkably reduced/eliminated leakage current.

Compared with the  $\text{CH}_3\text{NH}_3\text{PbI}_3$  perovskite, the excitons diffusion length and the charge mobility have been reported to be significantly improved by Cl doping in the  $\text{CH}_3\text{NH}_3\text{PbI}_{3-x}\text{Cl}_x$  perovskite.<sup>[4,5]</sup> Based on previous reports,<sup>[2,26]</sup> the Cl doping seems to play an important role in regulating the dynamics of exciton/charge carrier transport in the  $\text{CH}_3\text{NH}_3\text{PbI}_{3-x}\text{Cl}_x$  perovskite. Figure 2d shows a survey XPS spectrum for the  $\text{CH}_3\text{NH}_3\text{PbI}_{3-x}\text{Cl}_x$  perovskite. As can be seen, the XPS determined Cl atomic ratio is 8.3% for our  $\text{CH}_3\text{NH}_3\text{PbI}_{3-x}\text{Cl}_x$  perovskite, which is much higher than that of its solution-cast counterpart (1.4%),<sup>[23]</sup> though perovskite films with even a

higher Cl content could be obtained by a one-step deposition.<sup>[27]</sup> Although recent studies revealed that mixed halide has not always been formed in the perovskite materials generated from solution casting or thermal deposition.<sup>[28,29]</sup> The spectroscopic and XRD studies performed in this work demonstrated that there was no  $\text{PbCl}_2$  phase in our  $\text{CH}_3\text{NH}_3\text{PbI}_{3-x}\text{Cl}_x$  perovskite (Supporting Information, Figure S2), indicating that all the observed Cl elements were included as mixed phase in the  $\text{CH}_3\text{NH}_3\text{PbI}_{3-x}\text{Cl}_x$  perovskite (Figure S14 and S15 and associated discussions, Supporting Information). The higher Cl content could significantly improve the charge transport characteristics of the  $\text{CH}_3\text{NH}_3\text{PbI}_{3-x}\text{Cl}_x$  perovskite film fabricated by our layer-by-layer approach for high-performance photovoltaics.

The photovoltaic performance of the newly developed “multilayered”  $\text{CH}_3\text{NH}_3\text{PbI}_{3-x}\text{Cl}_x$  perovskite solar cells was measured under the simulated air mass 1.5 global (AM1.5G) solar irradiation. As shown in Figure 3, the open-circuit voltage ( $V_{oc}$ ), short-circuit current density ( $J_{sc}$ ), fill factor (FF), and PCE all depend strongly on the layer numbers. The corresponding device characteristics are given in Table 1, which shows a significantly increased  $V_{oc}$  from 0.53 V for the 1L device to 0.90 V for the 2L device. The starting small  $V_{oc}$  value (0.53 V, Figure 3a) was, most probably, caused by the thin perovskite layer with pinholes, resulting in the direct contact between PEDOT:PSS and PCBM with a leakage current (Figure S16, Supporting

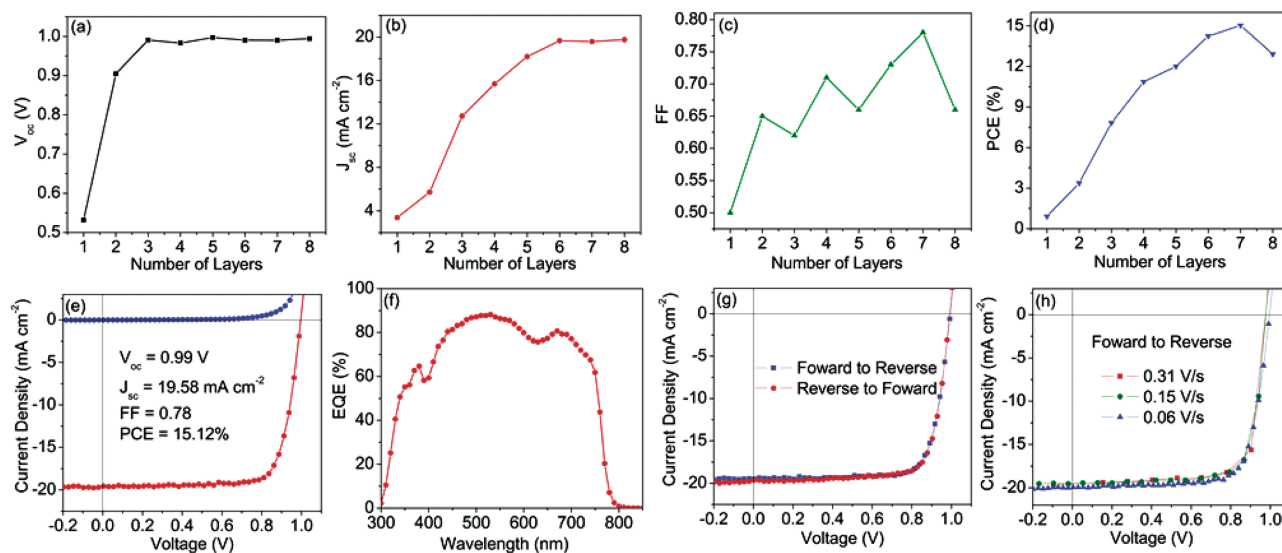


**Figure 3.** Device performance for  $\text{CH}_3\text{NH}_3\text{PbI}_{3-x}\text{Cl}_x$  perovskite solar cells with different layer numbers. a)  $V_{oc}$ , b)  $J_{sc}$ , c) FF, and d) PCE versus the layer numbers. e)  $J$ - $V$  characteristics measured under  $100 \text{ mW cm}^{-2}$  AM1.5G illumination (red) and in the dark (blue) for the device with an optimized layer number (7L). f) The corresponding EQE spectrum.  $J$ - $V$  curves for the device with an optimized layer number (7L): g) different scanning directions and h) different voltage sweep rates.

Information). As the layer number increased, the current leakage was effectively reduced/eliminated, and hence the rapidly increased  $V_{oc}$  (0.99 V) at around 3L and leveled off with further increase in the layer number. As seen in Figure 3b, the  $J_{sc}$  also gradually increased with increasing the layer number, but became saturated at  $\approx 20 \text{ mA cm}^{-2}$  around 6L, reflecting the sufficient absorption. On the other hand, FF increased from about 0.50 (1L) up to 0.78 (7L), and then decreased to 0.66 at 8L (Figure 3c). The apparently large FFs observed for the “multilayered”  $\text{CH}_3\text{NH}_3\text{PbI}_{3-x}\text{Cl}_x$  perovskite solar cells are resulted from the compact perovskite films formed by the layer-by-layer approach, leading to a balanced hole-electron transport and reduced charge recombination.<sup>[23]</sup> However, the presence of serious charge leakage in the thin 1L and charge recombination in the thick 8L devices led to the corresponding low FFs of 0.50 and 0.66, respectively. It is worthy to note that we used calcium (Ca) and aluminum (Al) as the cathode, which was demonstrated to be much better than the Al-only cathode with a typical S-shaped photocurrent profile of a very low FF (0.48)

**Table 1.** Performance parameters of the “multilayered”  $\text{CH}_3\text{NH}_3\text{PbI}_{3-x}\text{Cl}_x$  perovskite solar cells with different layer numbers.

Number of layers	$V_{oc}$ [V]	$J_{sc}$ [ $\text{mA cm}^{-2}$ ]	FF	PCE [%]
1	0.53	3.38	0.50	0.90
2	0.90	5.72	0.65	3.35
3	0.99	12.73	0.62	7.81
4	0.98	15.69	0.71	10.92
5	1.00	18.20	0.66	12.01
6	0.99	19.65	0.73	14.20
7	0.99	19.58	0.78	15.12
8	0.99	19.76	0.66	12.91

(Supporting Information, Figure S17). Therefore, the use of the Ca/Al cathode also made a significant difference.<sup>[22,23]</sup> Indeed, it has been reported that the different work functions of Ca and Al led to different interfacial properties with strong interfacial dipoles formed at the Ca/Al cathode,<sup>[30]</sup> which increased the charge extraction efficiency by reducing the charge extraction time and charge accumulation. Along with the increased  $V_{oc}$ ,  $J_{sc}$ , and FF with the layer number, the PCE also gradually increased with increasing the layer number up to the optimized 7L (Figure 3d). The current-voltage ( $J$ - $V$ ) characteristics measured under standard AM1.5G illumination and the corresponding external quantum efficiency (EQE) spectrum of the 7L device are shown in Figure 3e,f with the  $J_{sc}$ ,  $V_{oc}$ , FF, and PCE determined to be  $19.58 \text{ mA cm}^{-2}$ , 0.99 V, 0.78, and 15.12%, respectively. The PCE value of 15.12% for the 7L device is about 15 times higher than that of the 1L counterpart (0.90%) and among the top PCEs reported to date for perovskite solar cells with PCBM and PEDOT:PSS charge-transporting layers.<sup>[6,22,31,32]</sup>

The high EQE with a maximum value close to 88% highlighted the excellent performance of our  $\text{CH}_3\text{NH}_3\text{PbI}_{3-x}\text{Cl}_x$  perovskite solar cell (Figure 3f). The integrated short-circuit current from the EQE profile is  $18.93 \text{ mA cm}^{-2}$ , which is consistent well with the measured value of  $19.58 \text{ mA cm}^{-2}$ . The onset of photocurrent at 770 nm is also consistent with the absorption onset (Figure 2a) associated with the band gap of  $\text{CH}_3\text{NH}_3\text{PbI}_{3-x}\text{Cl}_x$  perovskite. For comparison, we also fabricated device by one-step solution casting a mixture of  $\text{PbCl}_2$  and  $\text{CH}_3\text{NH}_3\text{I}$  (1:3 mol/mol) in DMF according to reported procedures,<sup>[25]</sup> and found very poor device performance with the best  $J_{sc}$ ,  $V_{oc}$ , FF, and PCE of  $14.29 \text{ mA cm}^{-2}$ , 0.85 V, 0.67, and 8.14%, respectively (Supporting Information, Figure S18), though a relatively high FF could be obtained for films even with pinholes.<sup>[33]</sup>

Furthermore, Figure S19 in the Supporting Information shows that the PCE of the one-step solution-processed device

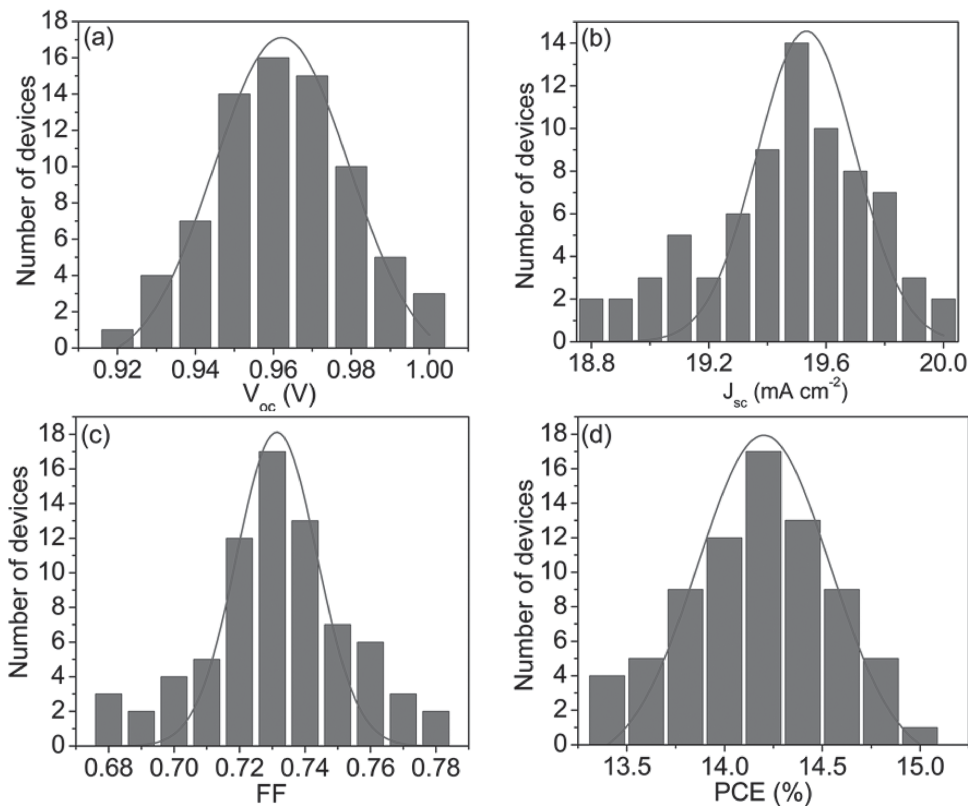


**Figure 4.** Histograms of device performance for 74  $\text{CH}_3\text{NH}_3\text{PbI}_{3-x}\text{Cl}_x$  perovskite solar cells. a)  $V_{oc}$ , b)  $J_{sc}$ , c) FF, and d) PCE measured for 74 individual devices.

dropped to 65% of its original value after storage in an Ar-filled glovebox without any device encapsulation for 30 d while the “multilayered”  $\text{CH}_3\text{NH}_3\text{PbI}_{3-x}\text{Cl}_x$  perovskite solar cell retained 95% of its original PCE under the same condition. The much better long-term stability observed for the  $\text{CH}_3\text{NH}_3\text{PbI}_{3-x}\text{Cl}_x$  perovskite solar cell fabricated by the layer-by-layer approach with respect to its one-step solution-cast counterpart can be attributed mainly to the more compact and highly crystalline “multilayered”  $\text{CH}_3\text{NH}_3\text{PbI}_{3-x}\text{Cl}_x$  perovskite film, leading to a much slower material degradation. Moreover, the device fabricated from the layer-by-layer approach showed a reduced leak current compared with the device made from solution casting, and hence a significantly reduced thermal-induced degradation for our perovskite.<sup>[11,17,34,35]</sup> As also can be seen in Figure S20 in the Supporting Information, the pristine  $\text{CH}_3\text{NH}_3\text{PbI}_{3-x}\text{Cl}_x$  perovskite film formed by the layer-by-layer approach exhibited slow degradation just at the film edge whereas the one-step solution-cast  $\text{CH}_3\text{NH}_3\text{PbI}_{3-x}\text{Cl}_x$  perovskite film degraded completely into  $\text{PbI}_2$  across the whole film after 21 d exposure in the ambient atmosphere. It has been reported that the substitution of larger I atoms in  $\text{CH}_3\text{NH}_3\text{PbI}_3$  with smaller Br atoms in  $\text{CH}_3\text{NH}_3\text{Pb}(\text{I}_{1-x}\text{Br}_x)_3$  perovskite could reduce lattice constant to significantly improve the perovskite film stability with increasing Br content.<sup>[17]</sup> Our  $\text{CH}_3\text{NH}_3\text{PbI}_{3-x}\text{Cl}_x$  perovskite film prepared by the layer-by-layer approach shows a much higher chlorine (Cl, which is even smaller than Br) content than that of its counterpart from the single-step solution process (8.3% vs 1.4% for the Cl atomic ratio – vide supra), and hence an

expected higher stability for the former. This, together with the reduced leak current and more compact morphology for the “multilayer”  $\text{CH}_3\text{NH}_3\text{PbI}_{3-x}\text{Cl}_x$  perovskite film (Figure S11, Supporting Information) with respect to its one-step solution-cast counterpart (Figure S12, Supporting Information), could rationalize the observed improved stability for the solar cell based on the  $\text{CH}_3\text{NH}_3\text{PbI}_{3-x}\text{Cl}_x$  perovskite fabricated by the layer-by-layer approach (Figure S19, Supporting Information), though detailed degradation mechanism deserves more in-depth investigation in follow up studies.

Perovskite solar cells in both mesoscopic<sup>[36]</sup> and planar junctions<sup>[37]</sup> have been demonstrated to show an anomalous hysteresis in the  $J$ - $V$  curves, making it difficult to accurately characterize the device performance. The scanning direction of the applied bias, voltage sweep rate, and light soaking and pre-conditioning of the device at a forward bias were all found to have a significant influence on the hysteresis,<sup>[38]</sup> which could cause either over or underestimated efficiency values. To ensure the accuracy of our characterization, we further investigated our devices in different scanning directions and at various voltage sweep rates. As can be seen in Figure 3g,h, our devices exhibited photocurrent hysteresis-free light  $J$ - $V$  curves with different scanning directions and/or voltage sweep rates. This indicates that the efficiencies measured for our  $\text{CH}_3\text{NH}_3\text{PbI}_{3-x}\text{Cl}_x$  perovskite solar cells with stable  $J$ - $V$  curves are reliable. The hysteresis-free characteristics of our devices can be attributed to low bulk/surface defect densities of the compact perovskite films formed by the layer-by-layer approach since these defects could act as

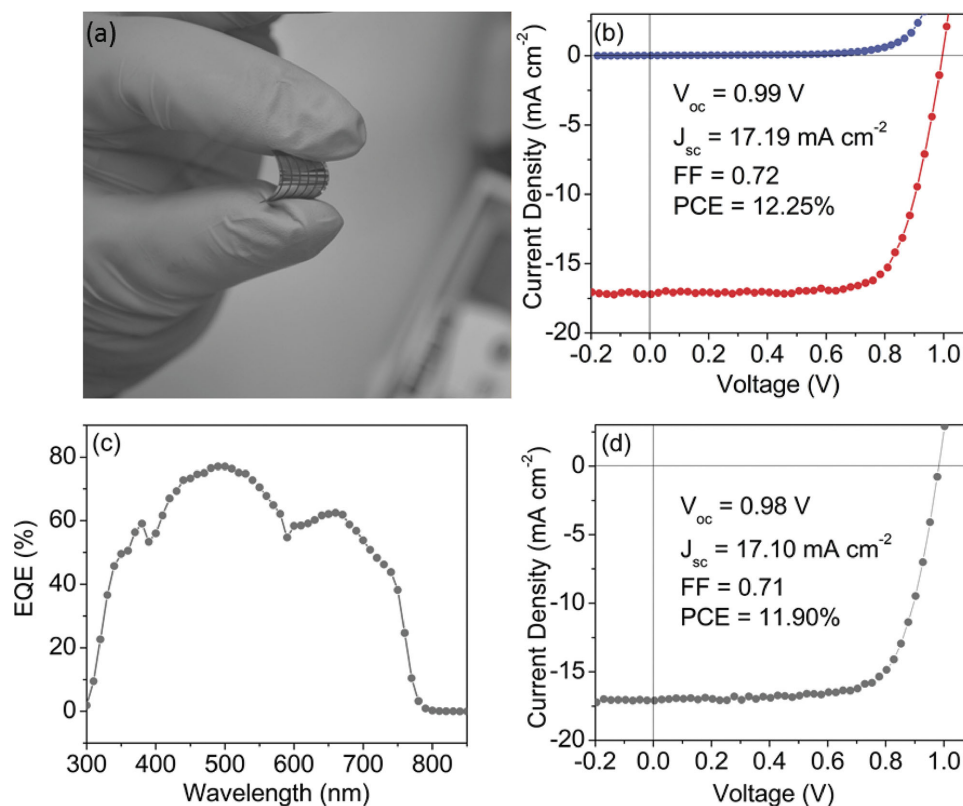


**Figure 5.** Device performance characteristics of flexible  $\text{CH}_3\text{NH}_3\text{PbI}_{3-x}\text{Cl}_x$  perovskite solar cell. a) Photograph of 7L flexible device prepared on a flexible ITO/PET substrate. b)  $J$ - $V$  characteristics measured under  $100 \text{ mW cm}^{-2}$  AM1.5G illumination (red) and in the dark (blue) for the 7L flexible device. c) EQE spectrum of the 7L flexible device. d)  $J$ - $V$  curve of the flexible device after being repeatedly bent for 1000 times.

traps for electrons and holes.<sup>[37]</sup> Possible contribution from the good interfaces between the perovskite films and charge-transporting layers (i.e., PEDOT:PSS, PCBM) cannot be ruled out as Xiao et al.<sup>[32]</sup> have also reported recently hysteresis-free devices based on the same charge-transporting layers of PEDOT:PSS and PCBM. Moreover, our results indicate that high-performance perovskite solar cells can be repeatedly fabricated using the layer-by-layer approach. Histograms of the  $V_{oc}$ ,  $J_{sc}$ , FF, and PCE of 74 individual devices using the optimized layer (7L) are given in Figure 4a–d, which show good reproducibility with a typical value of 0.98 V for  $V_{oc}$ ,  $19.50 \text{ mA cm}^{-2}$  for  $J_{sc}$ , 0.73 for FF, and over 14% for PCE for more than 85% of the devices.

The excellent performance discussed above prompted us to fabricate flexible solar cells by using the layer-by-layer approach to deposit  $\text{CH}_3\text{NH}_3\text{PbI}_{3-x}\text{Cl}_x$  perovskite onto the ITO-coated PET flexible substrate (Sigma–Aldrich). The  $J$ - $V$  curve of our flexible “multilayered” (7L)  $\text{CH}_3\text{NH}_3\text{PbI}_{3-x}\text{Cl}_x$  perovskite solar cell given in Figure 5a shows a  $V_{oc}$  of 0.99 V,  $J_{sc}$  of  $17.19 \text{ mA cm}^{-2}$ , FF of 0.72, and PCE of 12.25% (Figure 5b). To the best of our knowledge, the PCE of 12.25% is one of the highest values reported to date for all flexible perovskite solar cells.<sup>[7,13,23]</sup> The relatively low  $J_{sc}$  for the flexible  $\text{CH}_3\text{NH}_3\text{PbI}_{3-x}\text{Cl}_x$  perovskite device on the ITO/PET anode with respect to that of the ITO/Glass device is attributable to the relatively low EQE shown in Figure 5c with respect to that in Figure 3f. The EQE spectrum of the flexible device displays a low response at long wavelength associated with the low transmittance of the ITO/PET substrate

(Figure S21, Supporting Information), leading to a substantial loss of photocurrent in the 600–800 nm wavelength range. The newly developed flexible  $\text{CH}_3\text{NH}_3\text{PbI}_{3-x}\text{Cl}_x$  perovskite solar cell was subjected to bending test. As can be seen in Figure 5d, the device shows only an about 3% drop in efficiency even after having been repeatedly bent toward about 60° for 1000 times.

In summary, we have developed a layer-by-layer approach to uniform  $\text{CH}_3\text{NH}_3\text{PbI}_{3-x}\text{Cl}_x$  with desirable thickness for high performance and stable perovskite solar cells. The  $\text{CH}_3\text{NH}_3\text{PbI}_{3-x}\text{Cl}_x$  perovskite solar cells based on the ITO/Glass and flexible ITO/PET anodes exhibited PCEs with a champion of 15.12% and 12.25%, respectively; both are among the top values reported to date for respective devices. The observed superb device performances are attributable to the  $\text{CH}_3\text{NH}_3\text{PbI}_{3-x}\text{Cl}_x$  perovskite films with uniform morphologies and oriented crystalline domains formed by the newly developed layer-by-layer approach. This work represents a breakthrough in developing uniform  $\text{CH}_3\text{NH}_3\text{PbI}_{3-x}\text{Cl}_x$  perovskite films for highly efficient and stable perovskite solar cells of practical significance.

## Experimental Section

**Materials:** The PEDOT:PSS,  $\text{PbCl}_2$ , and PCBM were purchased from Clevious, Sigma-Aldrich, and Nano-C, respectively.  $\text{CH}_3\text{NH}_3\text{I}$  was synthesized according to reported procedures.<sup>[1]</sup>

*Electrical, Optical, and Microscopic Characterization of Films and Devices:* All measurements were carried out under ambient conditions. SEM images were taken on a Nova nanoSEM 600. UV-vis absorption was measured with a Shimadzu UV1800 spectrometer. XPS was measured on a VG Microtech ESCA 2000 using a monochromic Al X-ray source (97.9 W, 93.9 eV). Film thickness was measured by a KLA-Tencor P-6 Stylus profilometer.

*Device Fabrication:* ITO glass substrates were cleaned sequentially with detergent, deionized water, acetone, and isopropyl alcohol, followed by drying with N<sub>2</sub> flow and UV-ozone treatment for 15 min. The PEDOT:PSS solution (AI4083 from H. C. Starck) was spin-cast onto ITO electrodes at 5000 rpm for 40 s, followed by heating at 140 °C for 10 min. The PEDOT:PSS-coated ITO/Glass or ITO/PET substrate was then transferred to evaporator in an Ar-filled glovebox for PbCl<sub>2</sub> evaporation. Thereafter, the PbCl<sub>2</sub>-deposited substrate was dipped into a solution of CH<sub>3</sub>NH<sub>3</sub>I in 2-propanol (10 mg mL<sup>-1</sup>) for 40 s to form the CH<sub>3</sub>NH<sub>3</sub>PbI<sub>3-x</sub>Cl<sub>x</sub> perovskite and rinsed with 2-propanol. Similarly, a second PbCl<sub>2</sub> layer was thermally evaporated onto the CH<sub>3</sub>NH<sub>3</sub>PbI<sub>3-x</sub>Cl<sub>x</sub> perovskite film, followed by dipping into the CH<sub>3</sub>NH<sub>3</sub>I solution to form the second layer of CH<sub>3</sub>NH<sub>3</sub>PbI<sub>3-x</sub>Cl<sub>x</sub> perovskite, and the process repeated for several times until a desired thickness was obtained. The “multilayered” CH<sub>3</sub>NH<sub>3</sub>PbI<sub>3-x</sub>Cl<sub>x</sub> perovskite thus formed was then thermally annealed at 115 °C for 10 min in the glovebox to complete crystallization of the perovskite and to eliminate the interface, if any, through the film thickness. After the annealing, PCBM in chlorobenzene solution (17 mg mL<sup>-1</sup>) was deposited onto the perovskite layer by spin coating at 1000 rpm for 60 s. Finally, the device was transferred to the evaporator for thermal evaporation of Ca (20 nm) and Al (100 nm) at a pressure of 10<sup>-7</sup> Torr. The area of each device is 0.12 cm<sup>2</sup>, as defined by the overlap of the ITO and the thermally evaporated Al.

*Device Characterization:* All the devices were tested in an Ar-filled glovebox using a Keithley 2400 source meter and a Newport Oriel sol 2A solar simulator (300 W). The light intensity was calibrated to be 100 mW cm<sup>-2</sup> using a calibrated Si solar cell and a KG5 color filter. The device performance parameters were obtained from the *J*-*V* curves of the CH<sub>3</sub>NH<sub>3</sub>PbI<sub>3-x</sub>Cl<sub>x</sub> perovskite solar cells under illumination. The EQE was measured on a solar cell measurement system from PV Instruments Inc. We used the 91150V reference cell and meter (ORIEL Instruments) to calibrate the light intensity prior to the device testing.

Received: September 8, 2014

Revised: November 11, 2014

Published online:

- [1] M. M. Lee, J. Teuscher, T. Miyasaka, T. N. Murakami, H. J. Snaith, *Science* **2012**, *338*, 643.
- [2] C. Wehrenfennig, G. E. Eperon, M. B. Johnston, H. J. Snaith, L. M. Herz, *Adv. Mater.* **2014**, *26*, 1584.
- [3] V. D'Innocenzo, G. Grancini, M. J. P. Alcocer, A. R. S. Kandada, S. D. Stranks, M. M. Lee, G. Lanzani, H. J. Snaith, A. Petrozza, *Nat. Commun.* **2014**, *5*, 3586.
- [4] S. D. Stranks, G. E. Eperon, G. Grancini, C. Menelaou, M. J. P. Alcocer, T. Leijtens, L. M. Herz, A. Petrozza, H. J. Snaith, *Science* **2013**, *342*, 341.
- [5] G. C. Xing, N. Mathews, S. Sun, S. S. Lim, Y. M. Lam, M. Grätzel, S. Mhaisalkar, T. C. Sum, *Science* **2013**, *342*, 344.
- [6] O. Malinkiewicz, A. Yella, Y. H. Lee, G. M. Espallargas, M. Graetzel, M. K. Nazeeruddin, H. J. Bolink, *Nat. Photonics* **2014**, *8*, 128.
- [7] P. Docampo, J. M. Ball, M. Darwich, G. E. Eperon, H. J. Snaith, *Nat. Commun.* **2013**, *4*, 2761.
- [8] J. H. Heo, S. H. Im, J. H. Noh, T. N. Mandal, C.-S. Lim, J. A. Chang, Y. H. Lee, H.-J. Kim, A. Sarkar, M. K. Nazeeruddin, M. Grätzel, S. I. Seok, *Nat. Photonics* **2013**, *7*, 487.
- [9] B. V. Lotsch, *Angew. Chem. Int. Ed.* **2014**, *53*, 635.
- [10] A. Marchioro, J. Teuscher, D. Friedrich, M. Kunst, R. Krol, T. van de Moehl, M. Grätzel, J.-E. Moser, *Nat. Photonics* **2014**, *8*, 250.
- [11] J. N. Burschka, N. Pellet, S.-J. Moon, R. Humphry-Baker, P. Gao, M. K. Nazeeruddin, M. Grätzel, *Nature* **2013**, *499*, 316.
- [12] M. Z. Liu, M. B. Johnston, H. J. Snaith, *Nature* **2013**, *501*, 395.
- [13] D. Y. Liu, T. L. Kelly, *Nat. Photonics* **2014**, *8*, 133.
- [14] J. T. W. Wang, J. M. Ball, E. M. Barea, A. Abate, J. A. Alexander-Webber, J. Huang, M. Saliba, I. Mora-Sero, J. Bisquert, H. J. Snaith, R. J. Nicholas, *Nano Lett.* **2014**, *14*, 724.
- [15] H. Zhou, Q. Chen, G. Li, S. Luo, T.-B. Song, H.-S. Duan, Z. Hong, J. You, Y. Liu, Y. Yang, *Science* **2014**, *345*, 542.
- [16] N. J. Jeon, J. H. Noh, Y. C. Kim, W. S. Yang, S. Ryu, S. I. Seok, *Nat. Mater.* **2014**, *13*, 897.
- [17] J. H. Noh, S. H. Im, J. H. Heo, T. N. Mandal, S. I. Seok, *Nano Lett.* **2013**, *13*, 1764.
- [18] G. E. Eperon, S. D. Stranks, C. Menelaou, M. B. Johnston, L. M. Herz, H. J. Snaith, *Energy Environ. Sci.* **2014**, *7*, 982.
- [19] E. Edri, S. Kirmayer, D. Cahen, G. Hodes, *J. Phys. Chem. Lett.* **2013**, *4*, 897.
- [20] F. Hao, C. C. Stoumpos, D. H. Cao, R. P. H. Chang, M. G. Kanatzidis, *Nat. Photonics* **2014**, *8*, 489.
- [21] A. Mei, X. Li, L. Liu, Z. Ku, T. Liu, Y. Rong, M. Xu, M. Hu, J. Chen, Y. Yang, M. Grätzel, H. Han, *Science* **2014**, *345*, 295.
- [22] P.-W. Liang, C.-Y. Liao, C.-C. Chueh, F. Zuo, S. T. Williams, X.-K. Xin, J. Lin, A. K. -Y. Jen, *Adv. Mater.* **2014**, *26*, 3748.
- [23] J. B. You, Z. Hong, Y. Yang, Q. Chen, M. Cai, T.-B. Song, C.-C. Chen, S. Lu, Y. Liu, H. Zhou, Y. Yang, *ACS Nano* **2014**, *8*, 1674.
- [24] K. N. Liang, D. B. Mitzi, M. T. Prikas, *Chem. Mater.* **1998**, *10*, 403.
- [25] G. E. Eperon, V. M. Burlakov, P. Docampo, A. Goriely, H. J. Snaith, *Adv. Funct. Mater.* **2014**, *24*, 151.
- [26] C. Wehrenfennig, M. Liu, H. J. Snaith, M. B. Johnston, L. M. Herz, *Energy Environ. Sci.* **2014**, *7*, 2269.
- [27] B. Conings, L. Baeten, C. D. Dobbelaere, J. D'Haen, J. Manca, H.-G. Boyen, *Adv. Mater.* **2014**, *26*, 2041.
- [28] P. Docampo, F. C. Hanusch, S. D. Stranks, M. Döblinger, J. M. Feckl, M. Ehrensperger, N. K. Minar, M. B. Johnston, H. J. Snaith, T. Bein, *Adv. Energy Mater.* **2014**, *4*, 1400355.
- [29] Y. Zhao, K. Zhu, *J. Am. Chem. Soc.* **2014**, *136*, 12241.
- [30] X. Qiao, C. Zhao, B. Chen, L. Luana, B. Hu, *Org. Electron.* **2014**, *15*, 1624.
- [31] Z. Xiao, C. Bi, Y. Shao, Q. Dong, Q. Wang, Y. Yuan, C. Wang, Y. Gao, J. Huang, *Energy Environ. Sci.* **2014**, *7*, 2619.
- [32] Z. Xiao, Q. Dong, C. Bi, Y. Shao, Y. Yuan, J. Huang, *Adv. Mater.* **2014**, *26*, 6503.
- [33] G. E. Eperon, V. M. Burlakov, A. Goriely, H. J. Snaith, *ACS Nano* **2014**, *8*, 591.
- [34] J. A. Christians, R. C. M. Fung, P. V. Kamat, *J. Am. Chem. Soc.* **2014**, *136*, 758.
- [35] T. Leijtens, G. E. Eperon, S. Pathak, A. Abate, M. M. Lee, H. J. Snaith, *Nat. Commun.* **2013**, *4*, 2885.
- [36] A. Dualeh, T. Moehl, N. Tétreault, J. Teuscher, P. Gao, M. K. Nazeeruddin, M. Grätzel, *ACS Nano* **2014**, *8*, 362.
- [37] H. J. Snaith, A. Abate, J. M. Ball, G. E. Eperon, T. Leijtens, N. K. Noel, S. D. Stranks, J. T.-W. Wang, K. Wojciechowski, W. Zhang, *J. Phys. Chem. Lett.* **2014**, *5*, 1511.
- [38] E. L. Unger, E. T. Hoke, C. D. Bailie, W. H. Nguyen, A. R. Bowring, T. Heumüller, M. G. Christoforod, M. D. McGehee, *Energy Environ. Sci.* **2014**, *7*, 3690.